VYSOKÉ UČENÍ TECHNICKÉ V BRNĚ
BRNO UNIVERSITY OF TECHNOLOGY

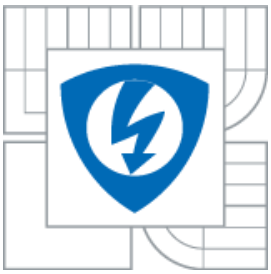

FAKULTA ELEKTROTECHNIKY A KOMUNIKAČNÍCH TECHNOLOGIÍ
ÚSTAV BIOMEDICÍNSKÉHO INŽENÝRSTVÍ

FACULTY OF ELECTRICAL ENGINEERING AND COMMUNICATION
DEPARTMENT OF BIOMEDICAL ENGINEERING

ADVANCED SIGNAL PROCESSING METHODS IN DYNAMIC CONTRAST ENHANCED MAGNETIC RESONANCE IMAGING

POKROČILÉ METODY ZPRACOVÁNÍ SIGNÁLŮ V ZOBRAZOVÁNÍ PERFÚZE MAGNETICKOU REZONANCÍ

ZKRÁCENÁ VERZE DIZERTAČNÍ PRÁCE
BRIEF VERSION OF PHD THESIS

AUTOR PRÁCE
AUTHOR
ING. MICHAL BARTOŠ

VEDOUCÍ PRÁCE
SUPERVISOR
ING. RADOVAN JIŘÍK, PH.D.

BRNO 2014

Abstract

This dissertation describes quantitative dynamic contrast enhanced magnetic resonance imaging (DCE-MRI), which is a powerful tool in diagnostics, mainly in oncology. After a time series of T_1-weighted images recording contrast-agent distribution in the body has been acquired, data processing phase follows. It is presented step by step in this dissertation. the theoretical background in physiological and MRI-acquisition modeling is described together with the estimation process leading to parametric maps describing perfusion and microcirculation properties of the investigated tissue on a voxel-by-voxel basis. the dissertation is divided into this theoretical analysis and a set of publications representing particular contributions of the author to DCE-MRI.

Keywords

Dynamic contrast enhanced MRI, perfusion, pharmacokinetic models, parameter estimation, deconvolution

Abstrakt

Tato dizertační práce představuje metodu zobrazování perfúze magnetickou rezonancí, jež je výkonným nástrojem v diagnostice, především v onkologii. Po ukončení sběru časové sekvence T_1-váhovaných obrazů zaznamenávajících distribuci kontrastní látky v těle začíná fáze zpracování dat, která je předmětem této dizertace. Je zde představen teoretický základ fyziologických modelů a modelů akvizice pomocí magnetické rezonance a celý řetězec potřebný k vytvoření obrazů odhadu parametrů perfúze a mikrocirkulace v tkáni. Tato dizertační práce je souborem uveřejněných prací autora přispívajícím k rozvoji metodologie perfúzního zobrazování a zmíněného potřebného teoretického rozboru.

Klíčová slova

DCE-MRI, perfúze, farmakokinetické modely, odhad parametrů, dekonvoluce

---

BARTOŠ, M. *Pokročilé metody zpracování signálů v zobrazování perfúze magnetickou rezonancí*. Brno: Vysoké učení technické v Brně, Fakulta elektrotechniky a komunikačních technologií, 2014. 73 s. Vedoucí dizertační práce Ing. Radovan Jiřík, Ph.D.

Dizertační práce je uložena na vědeckém oddělení děkanátu FEKT VUT v Brně, Technická 3058/10, 616 00 Brno.

CONTENTS

1 INTRODUCTION

1.1 QUANTITATIVE DYNAMIC CONTRAST ENHANCED MAGNETIC RESONANCE IMAGING

The quantitative dynamic contrast enhanced magnetic resonance imaging (DCE-MRI) is the topic of this thesis. DCE-MRI is a methodology, which consists of a series of estimation processes from the acquisition of the dynamic series of MRI images with contrast agent application to the formulation of parametric maps describing physiological properties of the tissue of interest. the physiological properties are parameters of a pharmacokinetic model. Based on the model used, it is possible to estimate plasma/blood flow, permeability of the capillary wall, volumes of plasma or extracellular extravascular spaces etc. These quantities, if estimated properly, are reproducible, allow inter- and intra-patient comparisons and describe undergoing physiological processes, which would allow us to make an inference about the state of the tissue, whether binary (physiological vs. pathological) or multary (diagnoses).

The standard DCE-MRI examination is done as follows. At the beginning, the subject (patient or animal) is placed into an MRI scanner and a scout images are acquired. After that a couple of native (pre-contrast) images is taken to allow further conversion of the data to the concentration of the contrast agent. Then the main acquisition starts to capture a sequence of T_1-weighted images with the time resolution in the range of 1 to 30 or more seconds. During this acquisition, when a few baseline pre-contrast images have been acquired, a gadolinium-based contrast agent is injected into the subject's vein as a short bolus. After a few minutes, during which the contrast agent has been distributing throughout the body, DCE-MRI processing starts, since all the necessary data have been collected. This processing phase is the scope of this dissertation and is presented below.

1.2 AIM OF THE DISSERTATION

The aim of this thesis was to contribute to a more widespread usage of the advanced processing methods in quantitative DCE-MRI including blind estimation of the arterial input function, the usage of complex pharmacokinetic models and precision description of the perfusion-parameter estimates. This can allow us to gain more information from the standard DCE-MRI acquisition.

The specific aims were:

1) To understand and remove convergence problems in nonlinear regression with adiabatic approximation of tissue homogeneity pharmacokinetic model (our reference [1] and **Paper I**)
2) To analyze and describe the precision of the perfusion-parameter estimates and to transfer this precision to the derived perfusion parameters (**Paper I**).

3) To enable processing of datasets with missing or corrupted arterial input function (crucial component of the pharmacokinetic model) by using blind deconvolution algorithm to estimate it (**Paper II**)
4) To contribute to application of these advanced processing methods in analysis of therapy response in oncology and validate these methods on relevant in-vivo data (**Paper III**)

2 MODELING

2.1 PHARMACOKINETIC MODEL

Any perfused part of the body can be in general described by a tissue unit given in Figure 2.1, where $C(t)$ is the molar concentration of an indicator (contrast agent) inside the modeled tissue (e.g. in mol/ml or M) and $J_{\text{in}}^{(i)}(t)$, $J_{\text{out}}^{(o)}(t)$ are fluxes (in mol/min/ml) into and out of the system, respectively. If it is assumed that the system is completely described by the tissue unit and that no indicator can disappear nor be created inside the unit, such a system can be described by the general principle of conservation of indicator mass [2]:

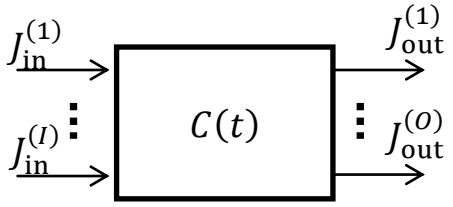

Figure 2.1: General tissue unit with *I* inlets and *O* outlets

$$\frac{dC(t)}{dt} = \sum_{i=1}^{I} J_{\text{in}}^{(i)}(t) - \sum_{o=1}^{O} J_{\text{out}}^{(o)}(t). \tag{2.1}$$

For linear and stationary (time-invariant) systems, the concept of transfer functions can be used. I.e. any output can be described as a linear combination of inputs:

$$J_{\text{out}}^{(o)}(t) = \sum_{i=1}^{I} J_{\text{in}}^{(i)}(t) * \eta^{(i,o)}(t) \tag{2.2}$$

where $\eta^{(i,o)}(t)$ is a transfer function or the probability distribution of transit times from the *i*-th input to the *o*-th output and $*$ is the convolution operator defined as:

$$f_1(t) * f_2(t) = \int_0^t f_1(u) f_2(t-u) du. \tag{2.3}$$

Because of the mass conservation principle or the fact that each $\sum_o \eta^{(i,o)}(t)$ is a probability density function of transit times, the function $\sum_o \eta^{(i,o)}(t)$ must fulfil the following: 1) the area is equal to 1; 2) all values are positive; 3) any $\eta^{(i,o)}(t < 0) = 0$, the system is causal.

2.1.1 Impulse residue function

After the substitution of (2.2) into (2.1) and finding the solution of such differential equation by integration with initial condition $C(t=0)=0$ (see appendix in [3]), the concentration of the indicator in the tissue unit can be written as:

$$C(t)=\sum_{i=1}^{I}\left(1-\int_{0}^{t}\sum_{o=1}^{O}\eta^{(i,o)}(t)\,dt\right)*J_{\mathrm{in}}^{(i)}(t)=\sum_{i=1}^{I}R_i(t)*J_{\mathrm{in}}^{(i)}(t) \tag{2.4}$$

where $R_i(t)$ is an impulse residue function (or impulse response function). Transforming the properties of $\sum_o \eta^{(i,o)}(t)$ from previous section, $R_i(t)$ is non-negative, non-increasing function with $R_i(t=0)=1$ and $lim\, R_i(t\to\infty)=0$. the impulse residue function describes the probability that a particle, which has entered the tissue unit, is still inside the unit at time instant t. Equivalently, it is a response of the system to the Dirac impulse at the arterial input. the flux in linear and stationary systems can be understood as a function of concentration, $J(t)=F\,c(t)$, where F is a rate constant also known as clearance (in ml/min/ml) and $c(t)$ is indicator concentration at the given input of the tissue unit. If F describes the transport of the contrast agent by convection, it is the flow of the carrier fluid normalized to the volume of the unit tissue. With the assumption of only one arterial inlet, (2.4) can be converted to the well-established model:

$$C(t)=R(t)*F_{\mathrm{p}}\,c_{\mathrm{a}}(t)=h(t)*c_{\mathrm{a}}(t) \tag{2.5}$$

where F_{p} is plasma flow (ml/min/ml) and $c_{\mathrm{a}}(t)$ is the arterial input function (AIF), i.e. concentration of the contrast agent in the feeding artery.

The basic quantitative parameters which can be extracted from $h(t)$ or $R(t)$ are plasma flow, F_{p}, mean transit time through the tissue unit, T (in min), and the fractional volume of the contrast-agent distribution space in the tissue unit, v (ml/ml). Since $R_i(t=0)=1$, F_{p} is equal to:

$$F_{\mathrm{p}}=h(0).. \tag{2.6}$$

The mean transit time through the system is:

$$T=\int_{0}^{\infty}R(t)dt \tag{2.7}$$

and using the central volume theorem [2], $v=F_{\mathrm{p}}T$:

$$v=\mathrm{F}\int_{0}^{\infty}R(t)dt=\int_{0}^{\infty}h(t)dt. \tag{2.8}$$

These physical quantities are usually connected with so called model-free analysis as no model is imposed to $R(t)$ or $h(t)$.

Another concept is called a model-based analysis [3] and assumes additional constraints on the possible form of $h(t)$, which is equivalent to the assumptions about the inner architecture of the general tissue unit in Figure 2.1. These assumptions are a compromise between physiological realism of the model and model complexity. Assuming that the indicator enters the modeled tissue only through one inlet, exits only through one outlet and can freely diffuse from plasma space to extracellular extravascular space (EES) or vice versa through the capillary wall which is symmetrically permeable, such a model can be graphically represented as Figure 2.2. the concentration of the indicator inside the whole unit is a weighted sum of the concentrations in each region:

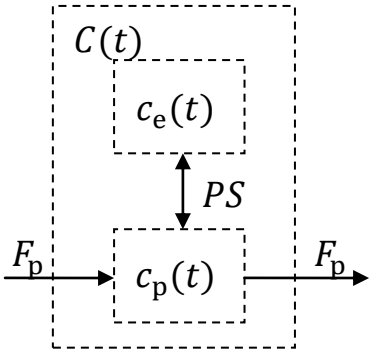

Figure 2.2: a non-specific tissue unit

$$C(t) = v_p c_p(t) + v_e c_e(t) \tag{2.9}$$

where v_p, v_e are (fractional) volumes of plasma and extravascular extracellular spaces (ml/ml), respectively and $c_p(t)$, $c_e(t)$ are the corresponding indicator concentrations.

Generalized kinetic model

One of the simplest models in tracer kinetic modeling is the so called generalized kinetic (GK) model [4] also known as the Tofts model [5] or the Kety model [6] according to the authors of the basic papers. the latter is one of the pioneering studies dating back to 1951.

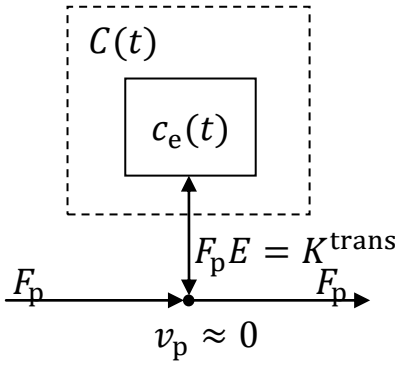

Figure 2.3: Generalized kinetic model

The model is based on the assumption that the tissue is weakly vascularized ($v_p \approx 0$) thus the whole plasma space can be excluded from the model (see Figure 2.3 in comparison with Figure 2.2). However, not all indicator passes from plasma to the EES compartment (as it could be in the case of a standard one compartment model) but only a fraction E of it (unitless or %). After substitutions to equation (2.1) and using (2.9) with $v_p = 0$, this model can be described by the standard ([4], [5], [7]) differential equation:

$$\frac{dC(t)}{dt} = K^{trans} c_a(t) - k_{ep} C(t) \tag{2.10}$$

where $K^{trans} = F_p E$ is the volume transfer constant and k_{ep} is rate constant between plasma and EES defined as:

$$k_{ep} = \frac{K^{trans}}{v_e}. \tag{2.11}$$

Using Laplace transform to solve (2.10) gives:

$$C(s) = \frac{K^{\text{trans}}}{s + k_{\text{ep}}} c_{\text{a}}(s) = h_{\text{GK}}(s) c_{\text{a}}(s). \tag{2.12}$$

Transforming this equation back to the time domain using inverse Laplace transform gives the known convolution formula (2.5) with the impulse residue function of the generalized kinetic model $h_{\text{GK}}(t)$:

$$C(t) = K^{\text{trans}} e^{-k_{\text{ep}} t} * \, c_{\text{a}}(t) = h_{\text{GK}}(t) * c_{\text{a}}(t). \tag{2.13}$$

Extended generalized kinetic model

The extended generalized kinetic (EGK) model [4] also referred to as the extended Tofts model [3], [5], [7] is the most widespread model in DCE imaging. It is the GK model where the assumption about the negligible plasma space is not used. the plasma space is included in the model, but not as a compartment, rather the plasma concentration $c_{\text{p}}(t)$ mimics the input concentration $c_{\text{a}}(t)$, see Figure 2.4.

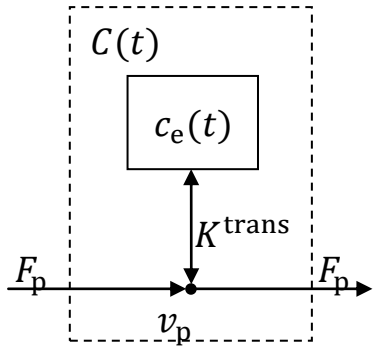

Figure 2.4: Extended generalized kinetic model

The derivation of the model is similar to the GK model except for the simplification ($v_{\text{p}} = 0$) of the equation (2.9). the differential equation has the same form as (2.10) and if it is solved together with (2.9) using the simplification $c_{\text{p}}(t) = c_{\text{a}}(t)$, it will lead to the following solution in the Laplace domain:

$$C(s) = \left(v_{\text{p}} + \frac{K^{\text{trans}}}{s + k_{\text{ep}}} \right) c_{\text{a}}(s) = h_{\text{EGK}}(s) c_{\text{a}}(s). \tag{2.14}$$

The transformation to the time domain is straightforward:

$$C(t) = \left(v_{\text{p}} \delta(t) + K^{\text{trans}} e^{-k_{\text{ep}} t} \right) * \, c_{\text{a}}(t) = h_{\text{EGK}}(t) * c_{\text{a}}(t) \tag{2.15}$$

but the interpretation of its impulse response $h_{\text{EGK}}(t)$ brings complications because of the Dirac impulse, $\delta(t)$.

Two compartment exchange model

The two compartment exchange model (2CXM) models both the plasma space and EES as compartments (Figure 2.5) thus it needs to be described by the system of two differential equations (2.16), (2.17). To find the concentration function of the whole tissue unit, it is necessary to substitute the solutions per each compartment into (2.9).

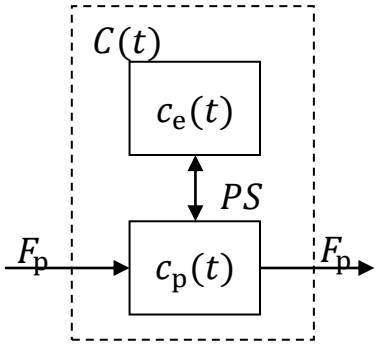

Figure 2.5: Two compartment exchange model (2CXM)

$$v_{\text{p}} \frac{dc_{\text{p}}(t)}{dt} = F_{\text{p}} c_{\text{a}}(t) - F_{\text{p}} c_{\text{p}}(t) + PS c_{\text{e}}(t) - PS c_{\text{p}}(t) \tag{2.16}$$

$$v_{\text{e}} \frac{dc_{\text{e}}(t)}{dt} = PS c_{\text{p}}(t) - PS c_{\text{e}}(t) \tag{2.17}$$

Using following substitutions for simplifications [2]:

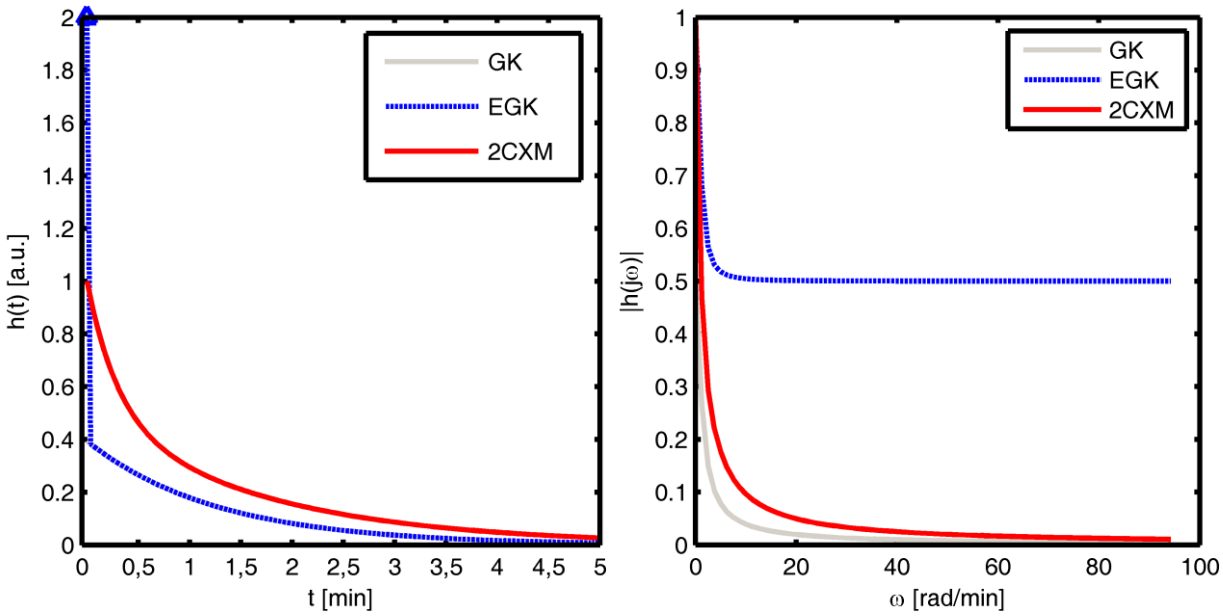

Figure 2.6: Typical shape of GK, EGK, 2CXM models in time (left) and Fourier amplitude (right) domains. the GK model coincides with the exponential part of the EGK model in time domain.

$$v_{\mathrm{p}} = F_{\mathrm{p}} T_{\mathrm{c}},\ PS = \frac{v_{\mathrm{e}}}{T_{\mathrm{e}}} \text{ and } v_{\mathrm{e}} = F_{\mathrm{p}}(T - T_{\mathrm{c}}) \tag{2.18}$$

where $T, T_{\mathrm{c}}, T_{\mathrm{e}}$ are mean transit times trough whole system, capillary plasma space and EES, respectively, the solution in the Laplace domain has the following form [2]:

$$C(s) = F_{\mathrm{p}} \frac{T + sT_{\mathrm{c}}T_{\mathrm{e}}}{s^2 T_{\mathrm{c}}T_{\mathrm{e}} + s(T + T_{\mathrm{e}}) + 1}\, c_{\mathrm{a}}(s) = h_{2\mathrm{CXM}}(s)\, c_{\mathrm{a}}(s). \tag{2.19}$$

The inverse Laplace transform gives the time-domain solution [2]:

$$C(t) = \frac{(T\,\alpha_- - 1)\,\alpha_- e^{-t\,\alpha_-} + (1 - T\,\alpha_-)\,\alpha_+ e^{-t\,\alpha_+}}{\alpha_+ - \alpha_-} * c_{\mathrm{a}}(t)$$
$$where: \alpha_{\pm} = \frac{T + T_{\mathrm{e}} \pm \sqrt{(T + T_{\mathrm{e}})^2 - 4\,T_{\mathrm{c}}T_{\mathrm{e}}}}{2T_{\mathrm{c}}T_{\mathrm{e}}}. \tag{2.20}$$

The direct solution of the equations (2.16), (2.17) without the substitution can be found in [4].

Tissue homogeneity model

The tissue homogeneity (TH) model was developed in [8]. Its main limitation is that it has no closed-form time-domain solution thus its applications were for a long time limited only to few studies [9], [10]. This was until the publication of the paper of Garpebring et al. [11] which has shown that the Laplace domain solution is sufficient to describe the model in the Fourier domain, together with the use of the inverse fast Fourier transform (FFT - see section 3.5.1). the example shapes of the TH impulse response in the Fourier domain and in time domain using FFT are plotted in Figure 2.10.

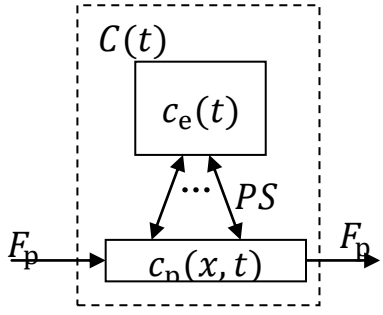

Figure 2.7: Tissue homogeneity (TH) model

The model is depicted in Figure 2.7 and its difference from the previous models lies in the modeling of the plasma space. the plasma space is no more understood as a well-mixed compartment but rather as a thin tube divided into infinitesimal subspaces which are not connected to its neighbors but are just constantly moving from the inlet to the outlet. the exchange of the indicator is allowed only between each subspace and the EES compartment. the physiological background behind is a blood flow through a thin capillary where red blood cells create "plugs" hence the name plug-flow for such plasma model.

The differential equations for the TH model are more complicated since the concentration $c_{\mathrm{p}}(x,t)$ depends also on the spatial position x along the capillary and can be found in many papers [3], [7], [8], [10], [11], however the derivation of the solution in the Laplace domain can be found only in the original paper [8]. the revised result in [2] has the form:

$$h_{\mathrm{TH}}(s) = \frac{(T + s\,T_{\mathrm{c}}T_{\mathrm{e}})(s\,T_{\mathrm{c}} + a)\left(1 - e^{-(s\,T_{\mathrm{c}}+a)}\right)}{s\,(T + s\,T_{\mathrm{c}}T_{\mathrm{e}})(s\,T_{\mathrm{c}} + a) + a\,(1 - e^{-(s\,T_{\mathrm{c}}+a)})} \qquad (2.21)$$
$$where: a = \frac{T - T_{\mathrm{c}}}{T_{\mathrm{e}}}.$$

Adiabatic approximation to the tissue homogeneity model

This model was developed in [12] and has quickly become popular for the estimation of plasma flow and capillary permeability [2], because unlike the TH model, it has a closed-form solution in the time domain.

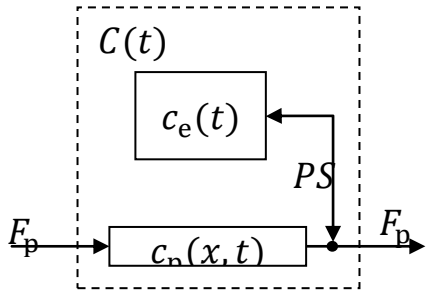

Figure 2.8: Adiabatic approximation to the tissue homogeneity (ATH) model

As the name of the model indicates, this model is an approximation of the TH model using the adiabatic condition, i.e. the capillary-wall permeability is negligible in the arterial phase of the indicator distribution. This comes from the assumption that the indicator concentration changes in the EES are much slower in comparison with the plasma space changes. the adiabatic approximation to the TH model (ATH) is depicted in Figure 2.8. the exchange between the plasma and EES takes place only at the end of the capillary and the capillary itself represents only a delay unit. the derivation of the model can be found in the original paper [12]. the differential equations and the Laplace- (2.22) and time-domain solutions are based on (or can be found in) [2]. the Laplace-domain solution is

$$h_{\mathrm{ATH}}(s) = F_{\mathrm{p}}\frac{1 - e^{-s\,T_{\mathrm{c}}}}{s} + \frac{F_{\mathrm{p}}E\,e^{-s\,T_{\mathrm{c}}}}{\frac{F_{\mathrm{p}}E}{v_{\mathrm{e}}} + s}. \qquad (2.22)$$

However the authors of [2] omitted to analyze the existence of this functional form. It is evident that (2.22) is not defined for $s = -F_{\mathrm{p}}E/v_{\mathrm{e}}$ and $s = 0$. the former one is unimportant since all the parameters are real and positive but the latter one is

crucial for the use with the inverse fast Fourier transform as proposed by [11] (see section 3.5.1). the definition of the ATH model for $s = 0$ can be found computing the limit:

$$h_{\mathrm{ATH}}(s = 0) = \lim_{s \to 0} h_{\mathrm{ATH}}(s) = v_{\mathrm{p}} + v_{\mathrm{e}}. \tag{2.23}$$

The same can be obtained intuitively since the zero (direct) component of a Laplace/Fourier-domain image is the area under the curve in the time domain, i.e. a sum of the plasma and EES volumes. the time-domain solution has the form:

$$h_{\mathrm{ATH}}(t) = F_{\mathrm{p}}\, \mathcal{H}(T_c - t) + \mathcal{H}(t - T_{\mathrm{c}})\, F_{\mathrm{p}} E\, e^{-\frac{F_{\mathrm{p}} E}{v_{\mathrm{e}}} t} = F_p \left(R_{\mathrm{p}}(t) + R_{\mathrm{e}}(t) \right) \tag{2.24}$$

where $\mathcal{H}(t)$ is the Heaviside (unit step) function, $R_{\mathrm{p}}(t)$ is the impulse response of the plasma space and $R_{\mathrm{e}}(t)$ is the impulse response of the EES.

Distributed parameter model

The original paper [13] describing the distributed parameter (DP) model was published in 1953, however its modern formulation in terms of impulse residue function for DCE-MRI studies starts with the paper [14].

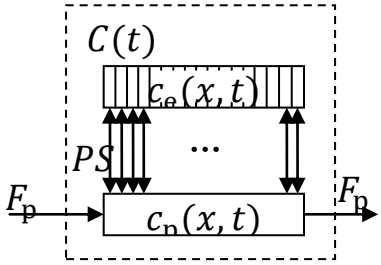

Figure 2.9: Distributed-parameter (DP) model

The plasma space is modeled as the plug-flow system as in the TH model but the indicator does not distribute from the capillary to the general EES compartment but to separate infinitesimal EES compartments, which are not interconnected to each other (see Figure 2.9). the consequence of it is that the indicator can only flow back to the position in the capillary, from where it has entered the EES. Hence the shortest path through the whole system, in comparison with the TH model, is through the capillary plasma space only.

The differential equation of the model can be found in [2], [4] but the derivation of the Laplace-domain solution needs to be found in [14]. After a few substitutions, it has the form [2]:

$$h_{\mathrm{DP}}(s) = F_{\mathrm{p}} \frac{1 - e^{-s \frac{T + s T_{\mathrm{c}} T_{\mathrm{e}}}{1 + s T_{\mathrm{e}}}}}{s}. \tag{2.25}$$

The function is not defined for $s = 0$ again so it is necessary to find the limit:

$$h_{\mathrm{DP}}(s = 0) = \lim_{s \to 0} h_{\mathrm{DP}}(s) = F_{\mathrm{p}} T = v_{\mathrm{p}} + v_{\mathrm{e}}. \tag{2.26}$$

The expression $F_{\mathrm{p}} T = v_{\mathrm{p}} + v_{\mathrm{e}}$ can be found using (2.18). the derivation of the time-domain solution can again be found in [14] (Equation (23a) and can be rewritten to [2]:

$$h_{\mathrm{DP}}(t) = 1 - \mathcal{H}(t - T_{\mathrm{c}}) e^{-\frac{T - T_{\mathrm{c}}}{T_{\mathrm{e}}}} \left(1 + \int_0^{T - T_{\mathrm{c}}} e^{-\frac{T}{T_{\mathrm{e}}}} \sqrt{\frac{T - T_{\mathrm{c}}}{t\, T_{\mathrm{e}}}} I_1 \left(2\sqrt{(T - T_{\mathrm{c}}) t} \right) \right) \tag{2.27}$$

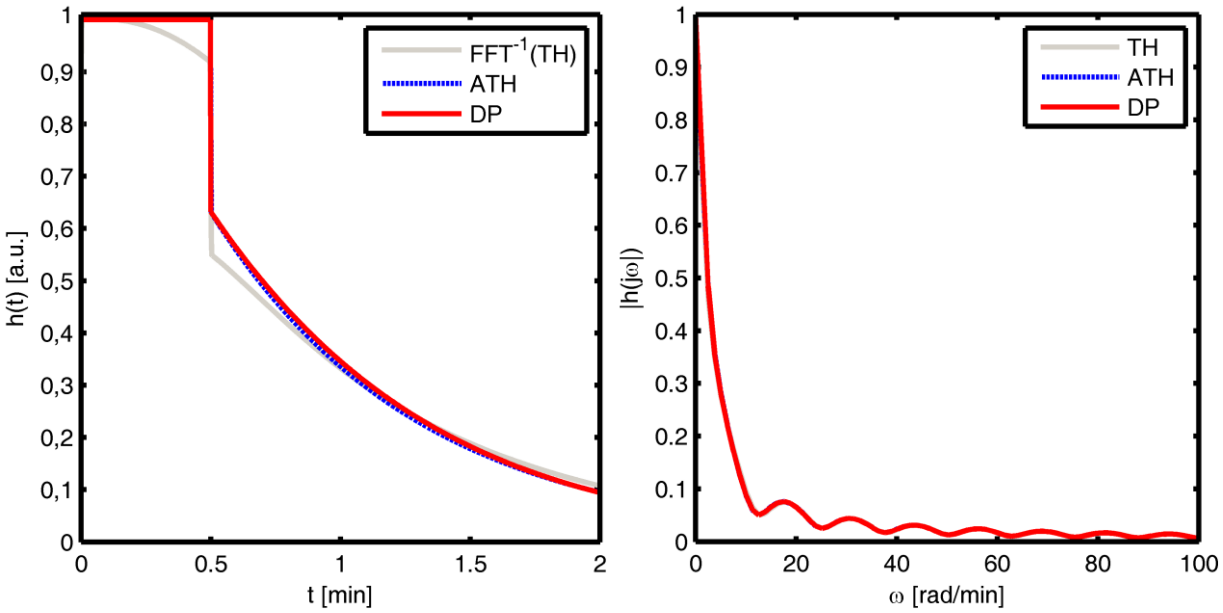

Figure 2.10: Typical shape of TH, ATH, DP models in time (left) and Fourier amplitude (right) domains. the DP model almost coincides with the ATH model in time domain and all the models coincide in Fourier domain.

where $I_1(x)$ is the first-order modified Bessel function of the first kind. As stated in [14], (2.27) needs numerical integration thus the author proposed a different description of $h_{\mathrm{DP}}(t)$ (see (23d) in [14]). However, since Garpebring et al. [11] has shown the use of Laplace domain solutions (section 3.5.1), the time-domain solution is not necessary.

Distributed capillary/multiple pathway models

These models have been presented by Koh et al. [15], [16] and were revised by Schabel [17]. They represent a special group, where there is not only one tissue unit in a model, but there are multiple tissue subunits on different pathways of the vascular tree which are modeled using the ATH model (i.e. each tissue unit being characterized by a given capillary transit time) and all together represent the model of a tissue unit. the probability of the given pathway (tissue subunit) is represented by the probability distribution of the capillary transit time $D(T_{\mathrm{c}};\boldsymbol{d})$, where $\boldsymbol{d}$ is a vector of parameters of the probability distribution. Incorporating this probability function into the standard theory of impulse residue function, Koh et al. [15] have introduced a formula for an impulse residue function of a distributed capillary model $R_{\mathrm{DC}}(t)$ as:

$$R_{\mathrm{DC}}(t) = 1 - \int_0^t D(T_{\mathrm{c}};\boldsymbol{d})dT_{\mathrm{c}} + \int_0^t R_{\mathrm{e}}(t)D(T_{\mathrm{c}};\boldsymbol{d})dT_{\mathrm{c}} \qquad (2.28)$$

where $R_{\mathrm{e}}(t)$ is the EES impulse residue function of the tissue subunit used in each pathway (see the ATH model in 0). the last summand in (2.28) describes the impulse response of the EES and the rest describes the impulse response of the plasma space. the impulse residue function is then parameterized by the perfusion parameters of the ATH model plus additional parameters, ***d,***

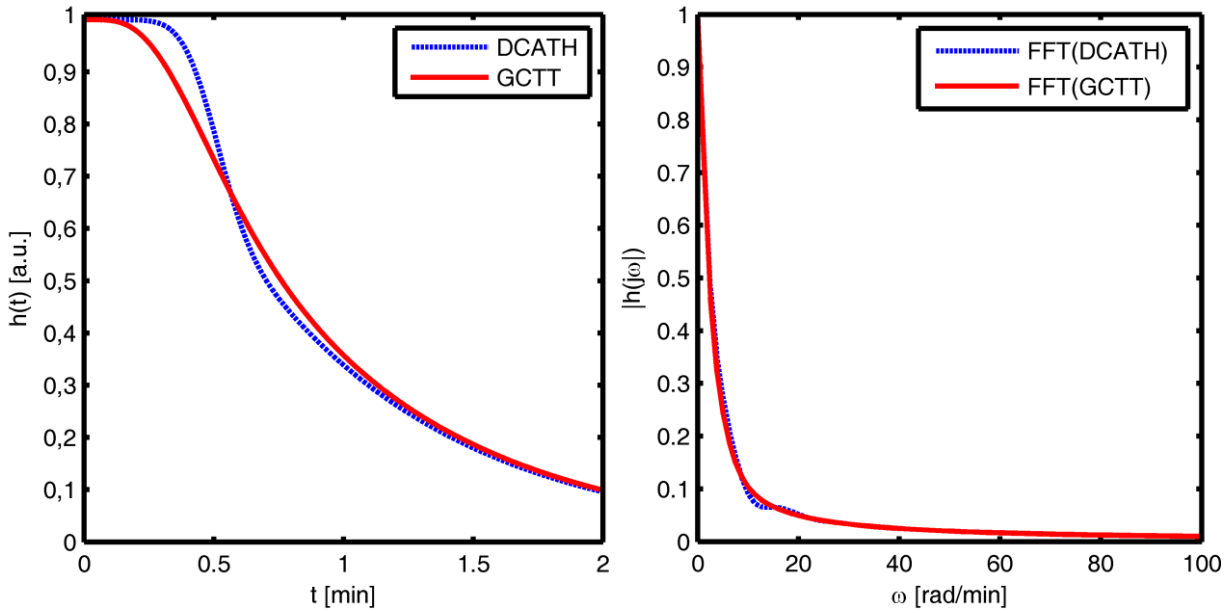

Figure 2.11: Typical shape of DCATH and GCTT models in time (left) and Fourier amplitude (right) domains. Both models are rendered using FFT in Fourier domain.

describing the probability distribution $D(T_c; \boldsymbol{d})$. For example if $D(T_c; d) = N(T_c; \sigma^2, \mu)$, i.e. the Gaussian distribution, it is one additional parameter σ.

In the original paper [15], the distributed capillary adiabatic tissue homogeneity (DCATH) model was introduced. Three distribution functions have been investigated: normal distribution, truncated normal distribution and skewed normal distribution; together with the ATH model as an elementary unit. the middle one has been used in **Paper I** and **Paper III** because it has no step between the plasma and EES phases (see section 3.5.1). Since the normal distribution is disputable from the physiological point of view, Schabel [17] has developed so called gamma capillary transit time (GCTT) model. the only difference lies in the gamma distribution instead of the normal one. But the breakthrough lies in its ability to unify the GK, EGK, ATH and 2CXM models. Hence, depending on its parameters, the GCTT model can represent any of the above models.

2.1.2 Arterial input function

It was shown in section 2.1.1 that the concentration of the indicator in a tissue can be described as convolution of the impulse residue function with an arterial input function (2.5), where the arterial input function (AIF) is the concentration of an indicator in a feeding artery of the investigated tissue. If the AIF has the form of a Dirac delta function, the concentration in the tissue is equal to the impulse residue function multiplied by F_p, i.e. $h(t)$.

Unfortunately, this ideal case is unreachable in perfusion experiments thus the AIF needs to be estimated. One possible way is to use mathematical models, which allow mathematical description of the AIF shape. However, the parameters of the model need to be setup properly so that the model approximates the real AIF. Hence, it is necessary to estimate the AIF parameters by an experiment.

Bi-exponential model

The bi-exponential model is well-known from the pharmacokinetic theory, thus it is the first candidate to use it for AIF modeling purposes. As shown in [18], it can well approximate the indicator kinetics but this study was intended for long time measurements (approx. an hour) with low temporal resolution, which is not appropriate for DCE-MRI applications (measurements done for several minutes). However, the model can still be used for dynamic short-time applications, but the time constants of the exponentials differ [19] from those obtained in [18]. This was pointed out in [20].

The model has a standard form [19]:

$$c_{\mathrm{a2}}(t) = A_{\mathrm{B}} e^{-\mu_{\mathrm{B}} t} + A_{\mathrm{G}} e^{-\mu_{\mathrm{G}} t} \tag{2.29}$$

where $A_{\mathrm{B}}, A_{\mathrm{G}}$ are scale constants, the sum $A_{\mathrm{B}} + A_{\mathrm{G}}$ gives the maximum of the (first) peak, and $\mu_{\mathrm{B}}, \mu_{\mathrm{G}}$ are decay constants of the fast and slow processes, respectively [21]. the time-domain description can be transformed to the Laplace domain to facilitate the computation of convolution giving:

$$c_{\mathrm{a2}}(s) = \frac{A_{\mathrm{B}}}{\mu_{\mathrm{B}} + s} + \frac{A_{\mathrm{G}}}{\mu_{\mathrm{G}} + s}. \tag{2.30}$$

Example shapes of the time- and frequency-domain representations is shown in Figure 2.12.

Gamma-variate model

The previous model does not take the initial rise of the bolus into account, because it is not designed for high sampling rates. This can be overcome using a gamma-variate function for the bolus function [19], which gives:

$$c_{\mathrm{a3}}(t) = A_{\mathrm{B}} t\, e^{-\mu_{\mathrm{B}} t} + A_{\mathrm{G}}(e^{-\mu_{\mathrm{G}} t} - e^{-\mu_{\mathrm{B}} t}). \tag{2.31}$$

This function can again be transformed to the Laplace domain:

$$c_{\mathrm{a3}}(s) = \frac{A_{\mathrm{B}}}{(\mu_{\mathrm{B}} + s)^2} - A_G\left(\frac{1}{\mu_{\mathrm{B}} + s} - \frac{1}{\mu_{\mathrm{G}} + s}\right) \tag{2.32}$$

The shape of the functions (without windowed version) is shown in Figure 2.12 for comparisons with other models.

Cosine model

Since the gamma-variate model suffers from discontinuities of the first derivative at $t = 0$, the authors of [19] have presented a different model with the raised cosine based bolus (see Figure 2.12). the physiological background for such function does not exist but still the model can approximate the measured AIFs quite well. And as stated in [19], this model can be used instead of Parker's AIF (see further) without significant loss in the accuracy of the parameter estimates of the impulse response function using EGK model (0). the closed-form solution in the time domain containing four parameters ($a_{\mathrm{B}}, a_{\mathrm{G}}, \mu_{\mathrm{B}}, \mu_{\mathrm{G}}$) can look complicated:

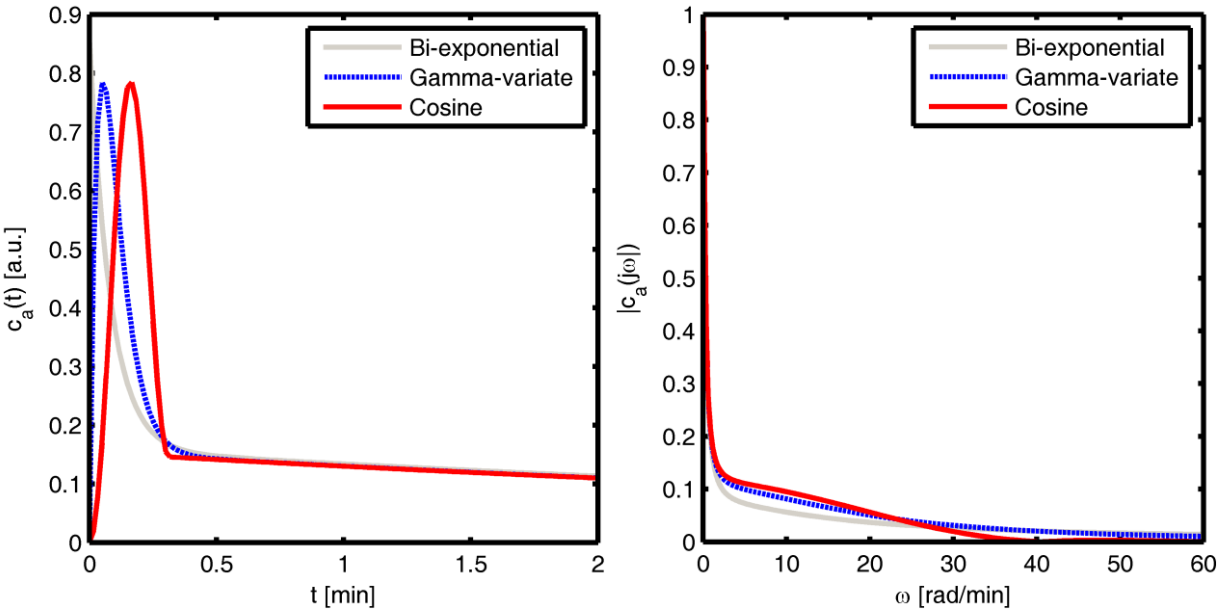

Figure 2.12: Typical shape of bi-exponential, gamma-variate and cosine models in time (left) and Fourier amplitude (right) domains.

$$c_{a4}(t) = \begin{cases} a_B(1-\cos(\mu_B t)) + \dfrac{a_B a_G}{\mu_G(1-e^{-\mu_G t})} - \\ \dfrac{a_B a_G}{(\mu_G^2+\mu_B^2)(\mu_G\cos(\mu_B t)+\mu_B\sin(\mu_B t)-\mu_G e^{-\mu_G t})} \end{cases}, 0 \le t \le \frac{2\pi}{\mu_B}$$
$$-a_B\, a_G \left(\frac{\mu_G - \mu_G e^{-\frac{2\pi\,\mu_G}{\mu_B}}}{\mu_B^2+\mu_G^2} + \frac{e^{-\frac{2\pi\,\mu_G}{\mu_B}} - 1}{\mu_G} \right) e^{-\mu_G\left(t-\frac{2\pi}{\mu_B}\right)}, t > \frac{2\pi}{\mu_B} \quad (2.33)$$

but it is not computationally demanding (as stated in [19]). However, it is possible to render this function through the Laplace domain, where the closed-form solution is simpler:

$$c_{a4}(s) = \begin{cases} -\dfrac{a_B\mu_B^2\left(e^{-\frac{2\pi s}{\mu_B}}-1\right)(a_G+\mu_G+s)}{s(\mu_G+s)(\mu_B^2+s^2)}, & s>0 \\ \dfrac{2\pi a_B(a_G+\mu_G)}{\mu_B\mu_G}, & s=0 \end{cases} \quad (2.34)$$

Parker model

This AIF was created for the approximation of a population averaged AIF [22] and has became a standard AIF for simulation purposes and studies, when other AIF estimate is not available. However, in the original study [22], the population averaged AIF was estimated using the indicator Gd-DTPA-BMA (Omniscan®), so this AIF model with parameter estimates from [22] should be used only for studies with this indicator.

This AIF has no physiological background and was designed by the authors of [22], which proposed to use two Gaussian functions for the first-pass and second-pass peaks and an exponential modulated by a sigmoid function to model the rest:

$$c_{\mathrm{P}}(t) = \sum_{n=1}^{2} \frac{A_n}{\sigma_n \sqrt{2\pi}} e^{-\frac{(t-T_n)^2}{2\sigma_n^2}} + \frac{\alpha e^{-\beta t}}{1 + e^{-g(t-\tau)}}. \tag{2.35}$$

Unfortunately, the transformation to the Laplace domain is not straightforward and was not found.

2.1.3 Delay and dispersion

The delay and dispersion are processes undergoing during the passage of the indicator through a vascular tree. They become problematic, if the AIF estimate is based on indicator concentration inside large artery (global AIF), because pharmacokinetic model (section 2.1) is based on the AIF corresponding to the small local feeding artery (local AIF). In that case, the global AIF should be corrected for delay and dispersion. the processes can be modeled as convolution of the global AIF with a vascular transport function (VTF) [23]:

$$c_{\mathrm{a}}^{\mathrm{loc}}(t) = h_{\mathrm{VTF}}(t) * c_{\mathrm{a}}^{\mathrm{glob}}(t) \tag{2.36}$$

where $c_{\mathrm{a}}^{\mathrm{loc}}(t), c_{\mathrm{a}}^{\mathrm{glob}}(t)$ are indicator concentrations in a local and global artery, respectively, and $h_{\mathrm{VTF}}(t)$ is the VTF, i.e. the vascular transit time distribution. the proper distribution $h_{\mathrm{VTF}}(t)$ is in general unknown but Calamante [23] has used computational fluid dynamics to validate three candidates defined analytically for dispersion modeling and has concluded, that the arterial tree can be modeled as one well-mixed compartment resulting in:

$$h_{\mathrm{VTF}}(t) = \frac{1}{T_{\mathrm{v}}} e^{-\frac{t}{T_{\mathrm{v}}}} \tag{2.37}$$

where T_{v} is the mean vascular transit time.

Incorporation of the delay into the model can be done using the substitution: $t \to t - t_{\mathrm{BAT}}$, where t_{BAT} is the so called bolus arrival time (BAT). If it is not necessary to consider the dispersion effect or if T_{v} is small, it is possible to use this substitution in any of the modeled function in (2.5), i.e. in the AIF or the impulse residue function to model only the delay of the AIF. However, if applied to a sampled discontinuous function (as usual for impulse residue function), there are substantial problems with the BATs (see also section 0), which are not equal to an integer multiple of the sampling interval as analyzed in [24] or in our contribution [1] and **Paper I**. a sampled function with non-integer BAT can in fact have same sample values as the same sampled function with the same but rounded BAT. This situation is unacceptable for usual minimization algorithms. Therefore we have advised to formulate the time-delay rather in the Fourier domain. This can be generalized to the Laplace transform resulting in:

$$f(t - t_{\mathrm{BAT}}) = f(t) * \delta(t - t_{\mathrm{BAT}}) = \mathcal{L}^{-1}\{f(s)\, e^{-t_{\mathrm{BAT}} s}\} \tag{2.38}$$

where f is any of the functions involved in the pharmacokinetic model (2.5).

2.2 CONTRAST-AGENT CONCENTRATION MODEL

The contrast agents for MRI applications are based on paramagnetic gadolinium-based substances which cause shortening of the longitudinal and transverse relaxation times T_1 and T_2 of the neighboring water molecules [25]. the usually used equation for this effect is [25]:

$$T_1^{-1} = T_{10}^{-1} + r_1 C \tag{2.39}$$

where T_{10} is the relaxation time of the tissue (background) without the presence of the contrast agent, C is the molar concentration of the contrast agent and r_1 is the relaxivity of the used contrast agent, which can be found in tables [26], [27]. This relation is also valid for T_2 (or transverse effective T_2^*) if the subscripts (and superscripts) are changed. However, T_2 (T_2^*) effects are usually assumed to be negligible in DCE-MRI (see section 3.3).

2.3 MODEL OF MRI SIGNAL

As stated in the previous section, contrast agent affects the relaxation times of water molecules. However, an MRI scanner does not measure these times directly but returns only a signal weighted by T_1 and/or T_2, T_2^*. This mathematical description of this weighting depends on the used MRI pulse sequence. the list of the suitable pulse sequences for DCE-MRI applications is quite limited. the fast two- or three-dimensional T_1-weighted spoiled gradient echo (SPGR) sequence is the most common technique [28]. the basic theoretical expression for the signal intensity when using this sequence is [29], [30]:

$$S(T_1, T_2^*) = M_0 \sin\theta \, e^{-\frac{TE}{T_2^*}} \frac{1 - e^{-\frac{TR}{T_1}}}{1 - \cos\theta \, e^{-\frac{TR}{T_1}}} \tag{2.40}$$

where TE, TR are the echo and repetition times, respectively; θ is the flip angle and M_0 is a constant dependent on proton density and the system gain.

The complete model relating the contrast-agent concentration to the MRI signal can be obtained by substituting (2.39) into (2.40):

$$\tilde{S}(t) = \varphi\big(\mathrm{C(t)}\big) = M_0 \sin\theta \, e^{-TE\left(T_{20}^{*\,-1} + r_2^* C(t)\right)} \frac{1 - e^{-TR\left(T_{10}^{-1} + r_1 C(t)\right)}}{1 - \cos\theta \, e^{-TR\left(T_{10}^{-1} + r_1 C(t)\right)}}. \tag{2.41}$$

3 ESTIMATION PROCESS

The whole previous section 2 was devoted to the modeling of the DCE-MRI data. the necessary models were introduced and then plug into each other to form a complete model for generation of MRI signal (2.41). However, the task of quantitative DCE-MRI is the inverse operation, i.e. an estimation of the perfusion parameters. In this section, a chain of estimation steps will be presented to allow proper estimation of the perfusion parameters.

3.1 SIGNAL MEASUREMENT

The first step in a DCE-MRI experiment starts with acquisition of data. Using an MRI scanner with a suitable pulse sequence (e.g. SPGR) provides us with a time-series of T_1-weighted images. Observing one voxel in time gives samples of estimates of the assumed model $\tilde{S}(t)$, which should be, in a simplified way, written as:

$$S(nT_s) = \delta(t - nT_s)\, w(t, (N-1)T_s)\, \tilde{S}(t) + \epsilon(n), \forall n = \{0,1, \dots N-1\} \quad (3.1)$$

where the Dirac function δ represents sampling points, w represents the measurement window defined as:

$$w(t, t_m) = \begin{cases} 1 & t \in \langle 0, t_m \rangle \\ 0 & elsewhere \end{cases} \quad (3.2)$$

where t_m is the duration of the measurement; and ϵ represents the measurement noise. the realizations of the random process, $\epsilon(n) \sim N(0, \sigma^2)$, can be described by the Gaussian distribution with zero mean and the standard deviation σ.

3.2 ESTIMATION OF TISSUE RELAXATION TIME T_{10} AND SCALING FACTOR M_0

Estimation of the contrast agent concentration is based on the model of the pulse sequence, (2.41) for SPGR, but this equation contain additional three unknowns: T_{10}, T_{20}^* and M_0, which must be also estimated for each voxel (the T_{20}^* term is neglected because it is negligible due to short *TE* and is hidden in M_0). For this purpose, DCE-MRI measurement process contains acquisition of a few images before the contrast-agent administration using several different flip angles [31] (see [30] for other techniques). the unknowns M_0 and T_{10} are then estimated by fitting of the non-linear model $S(T_{10}, T_{20}^*)$ (2.40) to the measured pre-contrast data. Since the non-linear regression is demanding, it can be substituted by a linear one using a method presented in [32].

3.3 ESTIMATION OF CONTRAST-AGENT CONCENTRATION

The following step in DCE-MRI is usually to convert the measured voxel-specific time signals $S(nT_s)$, where T_s is the sampling period and n is the time index, to the contrast-agent concentration time curves to simplify further processing. However this comfort simplification is controversial (see section 3.5) and if the full

equation for SPGR sequence is used (2.41), the income is disputable since the inversion $C(nT_s) = \varphi^{-1}(S(nT_s))$ must be solved numerically.

However, assuming negligible T_2^* effects (valid for short TE), the inversion has closed-form expression [29]:

$$C(nT_s) = \varphi_{\text{nl}}^{-1}\big(S(nT_s)\big) \approx \frac{1}{r_1}\left(\frac{1}{TR}\ln\left(\frac{(E_{10}-1)\Theta(nT_s)+E_{10}(1-\cos\theta)}{1+\cos\theta\big((E_{10}-1)\Theta(nT_s)-1\big)}\right)-T_{10}^{-1}\right), \forall n \quad (3.3)$$

where $E_{10} = e^{-\frac{TR}{T_{10}}}$ and:

$$\Theta(nT_s) = \frac{S(nT_s) - S(T_{10})}{S(T_{10})}. \quad (3.4)$$

The term $S(nT_s)$ is the complete measured signal recorded during the contrast-agent distribution, $S(T_{10})$ is the pre-contrast signal, which is usually estimated as an average of the samples of $S(nT_s)$ before the arrival of the contrast agent.

The non-linear function φ_{nl}^{-1} can even be approximated by a linear function $\varphi_{\text{lin}}^{-1}$ for low contrast-agent concentrations yielding [29]:

$$C(nT_s) = \varphi_{\text{lin}}^{-1}\big(S(nT_s)\big) \approx \frac{\Theta(nT_s)}{r_1 T_{10}}, \forall n. \quad (3.5)$$

This linear conversion is commonly used despite the fact, that it is not sufficiently accurate as shown in [28]. the use of the non-linear closed form solution (3.3) is justifiable but the numerical solution of (2.41) should be preferred [29]. the best option is, however, to directly estimate pharmacokinetic parameters from the signal, thus never explicitly solve for the concentration (see section 3.5).

3.4 ESTIMATION OF AIF

The fundamental problem in perfusion modeling is estimation of a suitable AIF. the accuracy of the AIF estimate is crucial, although many authors ignore this fact by shortly mentioning their source of AIF or not mentioning it at all. the possibilities how to estimate the AIF are presented shortly in this section.

Signal from voxel within artery

This standard technique is used in many practical studies. Signal intensity from a voxel within a (feeding) artery is converted to concentration as other voxels and used as the AIF. the benefit of this method is that it is possible to get individual (patient specific) AIFs. However, the measurement can be complicated, since it requires a suitable high-time-resolution acquisition protocol to properly sample the AIF in time, i.e. to follow the dynamics of the AIF and to avoid the acquisition-specific artifacts, such as partial volume [33] and inflow effects [34]. In addition, expert knowledge is needed to select a proper voxel if there is any present in the image at all.

Population average

If the dataset does not contain any suitable arterial voxel or the AIF is evidently distorted by acquisition artifacts and can not be repaired, use of a literature-based population averaged AIF may be a solution. the most popular form of a population based AIF was derived by Parker et.al. [22] and was presented in section 2.1.2. However, the population-based AIFs must be used carefully, since they are derived only for particular injection protocol and a particular contrast agent and should not be used in different situations.

Blind estimation

The last group of methods to estimate the AIF, when the previous ones are not possible or satisfactory, is blind estimation or identification of the AIF. This method is based on processing of only the measured tissue concentration curves. Since the model (2.5) contains convolution, it performs an inversion of this operation, i.e. deconvolution, without knowledge of the signal $h(t)$, hence also the term "blind deconvolution". Such a problem is in general ill-posed and needs additional information about the signals to be deconvolved. Such additional information is usually a certain type of smoothness imposed on the resulting signals or the convolution components are explicitly defined by a model, parameters of which are to be estimated. Since the method separates two components, both concepts can be combined. I.e. one component can be constrained by a model and the other one by a smoothing term. This was shown e.g. in [35] where they imposed polynomial smoothness on the AIF together with the extended general kinetic model. Another option used in [36], [37] and [38] is to constrain both curves by models. In that case it is necessary to solve a non-linear regression problem (see section 0).

The possibilities of AIF blind estimation were also investigated by our group and we have developed several blind estimation algorithms. the main contribution of our approach was that, to the best of our knowledge, we have been the first who applied more complex (and more realistic) models of the impulse residue function (ATH and DCATH) in the context of blind AIF estimation, compared to the so far used GK or EGK models.

The first method is single-channel deconvolution (**Paper II**) based on Lucy-Richardson deconvolution approach and the ATH model for impulse response function. the methodology was presented in **Paper II** and its application to a preclinical study of cancer treatment in **Paper III** and a conference [39].

3.5 ESTIMATION OF PHARMACOKINETIC PARAMETERS

The core of the dynamic contrast enhanced imaging is to estimate perfusion (and microcirculation) parameters of a tissue. the parameters define the shape of the impulse residue function, which is convolved with the AIF (2.5). If the AIF (or the parameters of it) is estimated in advance (section 3.4), the estimation process leads to a non-blind deconvolution problem. If not, it leads to blind deconvolution.

I.e. in blind deconvolution it is necessary to restore both the AIF and $h(t)$ from the measured signal and in non-blind deconvolution, only $h(t)$ needs to be restored.

The type of the restoration process is based on the definition of the convolution components. If they are defined analytically, using e.g. the models in sections 2.1.1 and 2.1.2, it is usually called the parametric approach (or model-based analysis) and its output are directly the parameters of interest. If the signals are defined by its samples, it is a non-parametric approach (or model-free analysis), which will return function(s) defined by the sample values. To estimate the perfusion parameters from a non-parametric impulse residue function, it is necessary to use the general properties described by (2.6)–(2.8). the estimated sampled impulse residue function can also be fitted by a model, which will form a combined method (**Paper II**).

For both approaches, the pharmacokinetic parameters $\boldsymbol{p}$ (or sample values, e.g. if $\boldsymbol{p} = \{h(nT_\mathrm{s})\}, \forall n$) are estimated by a general minimization process:

$$\arg\min_{\mathbf{p}} \psi(\varepsilon_1, \dots, \varepsilon_E) \tag{3.6}$$

where ψ is a criterial (or penalty, risk, ...) function and ε_e are error terms. the error term ε_1 is the so called data term and it is a difference between the measurement $S(nT_\mathrm{s})$ and a model $\hat{S}(nT_\mathrm{s})$:

$$\varepsilon_1(n) = S(nT_\mathrm{s}) - \hat{S}(nT_\mathrm{s}) = \tilde{S}(nT_\mathrm{s}) + \epsilon(n) - \hat{S}(nT_\mathrm{s}), \forall n \tag{3.7}$$

where $\tilde{S}(nT_\mathrm{s})$ stands for pure (true) signal and $\epsilon(n)$ is the measurement noise, i.e. a sequence of realizations of a random process described by its probability distribution (see section 3.1). the other error terms stand for additional information about the process and need not to be used. Even though the data term looks simple, it need not to be so, because as shown in section 2.3, $\hat{S}(nT_\mathrm{s})$ is not a function of the parameters of interest directly but it is a function of contrast-agent concentration. To get to the core of the model, i.e. to the pharmacokinetic model (2.5), it is necessary to apply a conversion function on one of the summand in (3.7). For practical purposes, the measured signal is usually converted to concentration, because it is possible to do the conversion in advance resulting in:

$$\varepsilon_1^\mathrm{C}(n) = \varphi^{-1}\big(\tilde{S}(nT_\mathrm{s}) + \epsilon(n)\big) - \hat{C}(nT_\mathrm{s}), \forall n \tag{3.8}$$

where φ^{-1} is an inversion of the signal generation process (e.g. (3.3) or (3.5)). the possible complication of such an approach is that $S(nT_\mathrm{s})$ contains a measurement noise and its distribution will be modified by such (nonlinear) conversion (see section 3.3). This can break the noise normality assumption (see section 3.5.2), thus the optimization process should be performed on the signal level, i.e.:

$$\varepsilon_1^\mathrm{S}(n) = \tilde{S}(nT_\mathrm{s}) + \epsilon(n) - \varphi\left(\hat{C}(nT_\mathrm{s})\right), \forall n \tag{3.9}$$

as also suggested by other authors [2], [25] and is supported by the analysis in [40].

3.5.1 Convolution integral

The core in the estimation of the perfusion parameters is the computation of the convolution integral, which operates on continuous functions. Because of the discrete nature of the MRI measurement (3.1) and the discrete computation environment, the discrete variants of the involved functions ($\hat{C}(nT_\mathrm{s}), \hat{h}(nT_\mathrm{s}), \widehat{c_\mathrm{a}}(nT_\mathrm{s})$) are to be used and the measured signal is approximated using discrete convolution:

$$\hat{C}(nT_\mathrm{s}) = \delta_\mathrm{W}(t - nT_\mathrm{s})\, \hat{C}(t) \approx \frac{1}{T_\mathrm{s}} \sum_{m=0}^{M-1} \hat{h}(mT_\mathrm{s})\, \widehat{c_\mathrm{a}}\big((n-m)T_\mathrm{s}\big) \tag{3.10}$$

where M is the number of samples of the AIF and δ_W is the discretization function. Because the computation of this sum is inefficient for signals longer than a few samples, it is usually replaced by the discrete Fourier transform and its inverse, both performed by Fast Fourier transform algorithm (FFT):

$$\hat{C}(nT_\mathrm{s}) = \hat{h}(nT_\mathrm{s}) * \widehat{c_\mathrm{a}}(nT_\mathrm{s}) = \frac{1}{\mathrm{T_s}} \mathrm{FFT}^{-1}\Big\{\mathrm{FFT}\big\{\hat{h}(nT_\mathrm{s})\big\}\, \mathrm{FFT}\{\widehat{c_\mathrm{a}}(nT_\mathrm{s})\}\Big\}, \forall n \tag{3.11}$$

where FFT^{-1} means the inverse FFT. However, this approach is performing circular convolution, so the input signals must be zero-padded before calling the FFT to have $N + M$ samples to avoid time-domain aliasing. the convolution output must then be cropped back to M valid samples.

As pointed out in [24], the approximation (3.10) is even insufficiently precise (see section 0), since the numerical integration is based on a basic rectangle rule, which is inappropriate for functions with steps (e.g. the ATH model of the impulse residue function, but generally every impulse residue function model has a step at $t = 0$). a relatively simple solution is to use a different numerical technique based on the trapezoidal rule as proposed in [24]. However, it is still an approximation.

A correct solution is to derive a closed-form formula for $\hat{C}(nT_\mathrm{s})$, which is possible only for some parametric models of both convolution components. the solution for the ATH model (2.24) and the AIF of the form (2.31) can be found in [24].

It is often not possible to derive a closed-form solution, e.g. because the AIF exists as a sampled signal or because the convolution integral simply does not have a closed-form solution. However, there is still an elegant solution coming from the deeper analysis of the convolution integral and the properties of the exponential transforms. the principle was published in [11] for the TH model but in the following text it will be generalized also for other models including the AIF models. the continuous-time-domain convolution can be rewritten to the Fourier domain:

$$\hat{C}(t) = \hat{h}(t) * \widehat{c_\mathrm{a}}(t) = \mathcal{F}^{-1}\Big\{\mathcal{F}\big\{\hat{h}(t)\big\}\, \mathcal{F}\{\widehat{c_\mathrm{a}}(t)\}\Big\} = \mathcal{F}^{-1}\big\{\hat{h}(j\omega)\, \widehat{c_\mathrm{a}}(j\omega)\big\}. \tag{3.12}$$

Substituting the Fourier transform by FFT for discrete signals simply yields (3.11), but using the relation between the Fourier transform and the Laplace

transform (i.e. the Fourier transform for causal signals is the Laplace transform if $s = j\omega$), (3.12) transforms to:

$$\hat{C}(t) = \mathcal{F}^{-1}\left\{\hat{h}(s)\,\widehat{c_{\mathrm{a}}}(s)\right\}\Big|_{s=j\omega}. \tag{3.13}$$

This equation can be rewritten for discrete signals using $\mathcal{F}^{-1} \rightarrow \mathrm{FFT}^{-1}$ and the sampled version of the signals spectra:

$$\begin{aligned}\hat{C}(nT_{\mathrm{s}}) &= w(t,(N-1)T_{\mathrm{s}})\,\hat{C}(t)\\ &= w(nT_{\mathrm{s}},(N-1)T_{\mathrm{s}})\,\mathrm{FFT}^{-1}\left\{\hat{h}(s)\,\widehat{c_{\mathrm{a}}}(s)\right\}\Big|_{s=kj\Delta\omega}, \forall n, \forall k\end{aligned} \tag{3.14}$$

where $\Delta\omega = \frac{2\pi}{K\,T_{\mathrm{s}}}$ and K is the number of samples after zero-padding needed to avoid time-domain aliasing, $k = \{0,1,\ldots K-1\}$, but its concrete form of k depends on the implementation of FFT algorithm. This approach allows an implementation of the impulse residue models described only in the Laplace domain as proposed in [11] for the TH model. But it can be beneficial for other models as well (e.g. the DP model which has a complicated time-domain solution containing Bessel function). the benefit of this approach also lies in the computation acceleration since the FFT is the most demanding operation and if the functions are rendered in the Fourier domain, it saves at least one computation of the FFT per iteration. the speed-up factor can be higher, because the computations of the gradients needed for the optimization algorithm are not taken into account.

3.5.2 Likelihood approach

Despite the general title of this section, it is devoted only to nonlinear regression using the non-linear least mean squares (LMS) method, which is the most common method in DCE-MRI. However, the corrected maximum likelihood estimator derived for non-Gaussian noise (3.8) has also been presented for DCE-MRI and compared to the LMS method [40].

To analyze all assumptions needed for the LMS method to find an unbiased estimate of the parameters is beyond the scope of this thesis and can be found elsewhere, e.g. in [41]. the important assumption is that the noise in the measurement must be normal with a constant variance. This is not valid in all DCE-MRI situations (e.g. because of nonlinear processing of the measured signal) and it is analyzed in [40].

The criterial function ψ in (3.6) for LMS has the form:

$$\psi(\boldsymbol{p}) = \sum_{o=1}^{O}\psi_o(\boldsymbol{p}_o) = \sum_{o=1}^{O}\sum_{n=0}^{N-1}\varepsilon_{1o}(nT_s,\boldsymbol{p}_o)^2 \tag{3.15}$$

where summation over O stands for observations, i.e. concentration curves in different tissues (voxels). If the curve-fitting is done independently as usual, then $O = 1$ and the sum disappears. the data term ε_{1o} is defined either by (3.8) or (3.9) with the difference, that it assumes an analytical model $\widehat{C_o}(nT_s,\boldsymbol{p}_o)$ and $\boldsymbol{p}_o$ is a vector of parameters in the particular tissue (voxel) to be found.

Traditional concept

The standard concept in DCE-MRI experiments supposes to have measured data already converted to represent the contrast-agent concentration (section 3.3) or that the measured signal intensity is directly proportional to the concentration. Furthermore, the AIF is estimated separately in advance (see section 3.4) and the measured signals are treated separately, voxel-by-voxel. Then,.(3.15) has the form:

$$\arg\min_{\boldsymbol{p}\in P}\sum_{n=0}^{N}\left(\varphi^{-1}\left(S(nT_{\mathrm{s}})\right)-\widehat{c_{\mathrm{a}}}(nT_{\mathrm{s}})*\hat{h}(nT_{\mathrm{s}},\boldsymbol{p})\right)^{2} \tag{3.16}$$

with the convolution integral usually solved using the FFT (3.11). This is not an optimal approach. As shown in [11], [24] and our paper [1], rendering discontinuous $\hat{h}(nT_{\mathrm{s}},\boldsymbol{p})$ in the time domain causes discontinuities in the criterial function, which leads to a failure in the minimization procedure, because the discontinuities cause local minima.

However, even if these induced minima would not be present (when a better computation technique for the calculation of the convolution is used, section 3.5.1), other local minima could be present, because it is a general problem in non-linear regression [41].

Assuming that the proper minimum has been selected, it is important (and in the literature mostly ignored) to estimate the confidence intervals of the estimated perfusion parameters. It can be based on characterization of the shape of the criterial function around the solution. This can be done by estimation of the covariance matrix from the gradients of the fitted model [41]. Although it is only an approximation of the true probability distribution of the estimates by the multivariate normal distribution, it can be very useful. This issue was investigated in **Paper I**.

Blind estimation

The blind estimation methods are based on simultaneous estimation of the parameters of both convolution components, i.e. the AIF and the impulse residue function. Adopting (3.15) for general blind LMS estimation results in:

$$\arg\min_{\substack{\boldsymbol{p}_o\in P,\forall o\\ \boldsymbol{p}_{\mathrm{a}}\in P_{\mathrm{a}}}}\sum_{o=0}^{O}\sum_{n=0}^{N}\left(\varphi^{-1}\left(S_o(nT_{\mathrm{s}})\right)-\widehat{c_{\mathrm{a}}}(nT_s,\boldsymbol{p}_{\mathrm{a}})*\hat{h}(nT_{\mathrm{s}},\boldsymbol{p}_o)\right)^{2} \tag{3.17}$$

where $\boldsymbol{p}_{\mathrm{a}}$ is the vector of parameters of the AIF model, $\boldsymbol{p}_o$ is a vector of parameters of the impulse residue function of the o^{th} tissue (voxel), $S_o(nT_s)$ is the measured signal in the o^{th} tissue (voxel) and P, P_{a} stands for the domains of definitions (i.e. constrains) for the parameters of the impulse response function and the AIF, respectively. the main idea behind this concept is that multiple tissues share the same AIF. Several variants of blind multichannel deconvolution have been presented by the group of di Bella [36], [37], [38], [42], [43] with the EGK model

and a special AIF with 11 parameters based on gamma-variate functions. Promising results were also presented by our group with the DCATH model and Parker's AIF [44], [45].

A special problem in blind estimation is the scale of the AIF or equivalently, the scale of the impulse residue function, since the scaling factors of these functions are inversely proportional. a possible solution of this problem is to scale the AIF estimate using a measurement of the AIF tail as suggested in [42] or using a literature-based perfusion-parameter (e.g. plasma volume + EES volume) in a reference tissue as used in **Paper III**.

3.5.3 Bayesian approach

Another approach to estimation of the impulse residue function or its parameters is based on Bayesian inference. the general concept of the estimation is similar (beginning of section 3.5), but the theoretical background is different and it is beyond the scope of this thesis to describe differences and possible similarities, which may arise.

Non-parametric approach

At the early phase of DCE-MRI (or rather DSC-MRI), standard estimators known from general signal processing theory were used, such as singular volume decomposition (SVD), [46], [47], Wiener filter [48] or Lucy-Richardson **Paper II**. Because the complete signal needs to be estimated from noisy data, these methods were not sufficiently robust. Hence, they were extended by an a priori knowledge about the signals, such as smoothness and monotonicity (in case of the impulse response function) to reduce their sensitivity to noise. Many authors have presented their regularization variants of the Tichonov regularization [23], [49], penalized monotonicity [46], constrained monotonicity [50], monotonicity constrained splines [51]or penalty B-splines [52]. the regularization possibilities are well analyzed by Keeling et al. in [53] or [54], where they have presented estimation of the impulse response function using an exponential basis.

Unlike the [54], these methods are model-free in the sense of physiological models described in (section 2.1.1). the possibility of imposing model-based regularization on deconvolution was shown by our group in **Paper II**, where we have presented an alternating minimization scheme with Lucy-Richardson deconvolution using total variation regularization and adiabatic tissue homogeneity model for blind estimation.

SELECTED PAPERS

Paper I

The precision of DCE-MRI using the tissue homogeneity model with continuous formulation of the perfusion parameters

Michal Bartoš, Radovan Jiřík, Jiří Kratochvíla, Michal Standara, Zenon Starčuk, Torfinn Taxt

Abstract

The present trend in dynamic contrast-enhanced MRI is to increase the number of estimated perfusion parameters using complex pharmacokinetic models. However, less attention is given to the precision analysis of the parameter estimates. In this paper, the distributed capillary adiabatic tissue homogeneity pharmacokinetic model is extended by the bolus arrival time formulated as a free continuous parameter. With the continuous formulation of all perfusion parameters, it is possible to use standard gradient-based optimization algorithms in the approximation of the tissue concentration time sequences. This new six-parameter model is investigated by comparing Monte-Carlo simulations with theoretically derived covariance matrices. the covariance-matrix approach is extended from the usual analysis of the primary perfusion parameters of the pharmacokinetic model to the analysis of the perfusion parameters derived from the primary ones. the results indicate that the precision of the estimated perfusion parameters can be described by the covariance matrix for signal-to-noise ratio higher than ~20dB. the application of the new analysis model on a real DCE-MRI data set is also presented.

Reference:

Bartoš M, Jiřík R, Kratochvíla J, Standara M, Starčuk Z, Taxt T. the precision of DCE-MRI using the tissue homogeneity model with continuous formulation of the perfusion parameters. Magn Reson Imaging 2014;32:505–13.
Available online:
http://www.sciencedirect.com/science/article/pii/S0730725X14000460

Paper II

Single-channel blind estimation of arterial input function and tissue impulse response in DCE-MRI

Torfinn Taxt, Radovan Jiřík, Cecilie Brekke Rygh, Renate Grüner, Michal Bartoš, Erling Andersen,Fitz-Roy Curry and Rolf K. Reed

Abstract

Multipass dynamic MRI and pharmacokinetic modeling are used to estimate perfusion parameters of leaky capillaries. Curve fitting and nonblind deconvolution are the established methods to derive the perfusion estimates from the observed arterial input function (AIF) and tissue tracer concentration function. These nonblind methods are sensitive to errors in the AIF, measured in some nearby artery or estimated by multichannel blind deconvolution. Here, a single-channel blind deconvolution algorithm is presented, which only uses a single tissue tracer concentration function to estimate the corresponding AIF and tissue impulse response function. That way, many errors affecting these functions are reduced. the validity of the algorithm is supported by simulations and tests on real data from mouse. the corresponding nonblind and multichannel methods are also presented.

Reference:

Taxt T, Jiřík R, Rygh CB, Grüner R, Bartoš M, Andersen E, et al. Single-channel blind estimation of arterial input function and tissue impulse response in DCE-MRI. IEEE Trans Biomed Eng 2012;59:1012–21.
Available online: *http://dx.doi.org/10.1109/TBME.2011.2182195*

Paper III

Anti-VEGF treatment reduces blood supply and increases tumor cell invasion in glioblastoma

Olivier Keunen, Mikael Johansson, Anaïs Oudin, Morgane Sanzey, Siti A. Abdul Rahim, Fred Fack, Frits Thorsen, Torfinn Taxt, Michal Bartos, Radovan Jirik, Hrvoje Miletic, Jian Wang, Daniel Stieber, Linda Stuhr, Ingrid Moen, Cecilie Brekke Rygh, Rolf Bjerkvig, and Simone P. Niclou

Abstract

Bevacizumab, an antibody against vascular endothelial growth factor (VEGF), is a promising, yet controversial, drug in human glioblastoma treatment (GBM). Its effects on tumor burden, recurrence, and vascular physiology are unclear. We therefore determined the tumor response to bevacizumab at the phenotypic, physiological, and molecular level in a clinically relevant intracranial GBM xenograft model derived from patient tumor spheroids. Using anatomical and physiological magnetic resonance imaging (MRI), we show that bevacizumab causes a strong decrease in contrast enhancement while having only a marginal effect on tumor growth. Interestingly, dynamic contrast-enhanced MRI revealed a significant reduction of the vascular supply, as evidenced by a decrease in intratumoral blood flow and volume and, at the morphological level, by a strong reduction of large- and medium-sized blood vessels. Electron microscopy revealed fewer mitochondria in the treated tumor cells. Importantly, this was accompanied by a 68% increase in infiltrating tumor cells in the brain parenchyma. At the molecular level we observed an increase in lactate and alanine metabolites, together with an induction of hypoxia-inducible factor 1α and an activation of the phosphatidyl-inositol-3-kinase pathway. These data strongly suggest that vascular remodeling induced by anti-VEGF treatment leads to a more hypoxic tumor microenvironment. This favors a metabolic change in the tumor cells toward glycolysis, which leads to enhanced tumor cell invasion into the normal brain. the present work underlines the need to combine anti-angiogenic treatment in GBMs with drugs targeting specific signaling or metabolic pathways linked to the glycolytic phenotype.

Reference:

Keunen O, Johansson M, Oudin A, Sanzey M, Rahim SAA, Fack F, et al. Anti-VEGF treatment reduces blood supply and increases tumor cell invasion in glioblastoma. Proc Natl Acad Sci U S a 2011;108:3749–54.
Available online: *http://www.pnas.org/content/108/9/3749*

4 CONCLUSION

The first part of this dissertation describes the necessary theoretical background for quantitative DCE-MRI. This part should contribute to understanding of our contribution made and described in the presented papers. DCE-MRI includes a chain of estimations from measuring of the MRI signal to the estimation of perfusion and microcirculation tissue parameters, which is the goal of quantitative DCE-MRI. the described chain was also transformed to a computer application, implemented by our group in the Matlab (Mathworks, Inc., Natic, US-MA) environment. This has contributed to a comfortable processing of datasets used not only in the presented papers in the second part of the dissertation.

Paper I contains two major contributions. First, a novel method for elimination of the step-wise discontinuous character of the criterial function to be minimized was proposed. This discontinuity is caused by the initial step of the impulse residue functions at the bolus arrival time (any model) and at the end of the vascular distribution phase (ATH and DP models). Analysis of this problem was also presented in our conference contribution [1] and in papers of other authors [11], [24]. We have solved this problem by performing the time-shift of the model in the Fourier domain and by using the DCATH model of the impulse residue function as presented in **Paper I**.

The second contribution in **Paper I** is our method for calculation of precision of the perfusion-parameter estimates. This is of great importance for the DCE-MRI studies, because reliable conclusions from the perfusion-parameter estimates can be drawn only when their confidence intervals are known.

Paper II is a result of collaboration with professor Torfinn Taxt. the underlying work of this paper started during my one-semester stay at his institution (University of Bergen). the main contribution of this paper is to allow processing of DCE-MRI datasets without having measured the arterial input function, and thus avoiding the related measurement artifacts. This could be done using blind deconvolution techniques. Namely using the Lucy-Richardson alternating minimization (also analyzed in our conference contribution [55]) with imposed analytical model of the impulse residue function and total variation regularization as presented in **Paper II**.

Another possibility to the blind estimation of the AIF is nonlinear regression. This is presented in our contributions [44], [45], [56] and [57], which are based on the extended DCATH model from **Paper I** and complex model-based AIFs.

All the concepts presented in **Paper I** and **Paper II** were used in a preclinical study of anti-angiogenic (reduction of tumor-vasculature growth) therapy response of glioblastoma presented in **Paper III**. We have shown on animal models that quantitative DCE-MRI is a powerful tool for assessment of perfusion and microcirculation of tumor environment. This was cross-validated with other methods such as histology, since this is still the only way to validate the new information gained from improved DCE-MRI.

REFERENCES

[1] Bartoš M, Keunen O, Jiřík R, Bjerkvig R, Taxt T. Perfusion Analysis of Dynamic Contrast Enhanced Magnetic Resonance Images Using a Fully Continuous Tissue Homogeneity Model with Mean Transit Time Dispersion and Frequency Domain Estimation of the Signal Delay. Anal Biomed Signals Images 2010;20:269–74.

[2] Sourbron SP, Buckley DL. Tracer kinetic modelling in MRI: estimating perfusion and capillary permeability. Phys Med Biol 2011;57:R1–R33.

[3] Sourbron SP, Buckley DL. Classic models for dynamic contrast-enhanced MRI. NMR Biomed 2013;26:1004–27.

[4] Koh TS, Bisdas S, Koh DM, Thng CH. Fundamentals of tracer kinetics for dynamic contrast-enhanced MRI. J Magn Reson Imaging 2011;34:1262–76.

[5] Tofts PS, Brix G, Buckley DL, Evelhoch JL, Henderson E, Knopp M V, et al. Estimating kinetic parameters from dynamic contrast-enhanced T(1)-weighted MRI of a diffusable tracer: standardized quantities and symbols. J Magn Reson Imaging 1999;10:223–32.

[6] Kety SS. the theory and applications of the exchange of inert gas at the lungs and tissues. Pharmacol Rev 1951;3:1–41.

[7] Sourbron SP, Buckley DL. On the scope and interpretation of the Tofts models for DCE-MRI. Magn Reson Med 2011;66:735–45.

[8] Johnson JA, Wilson TA. a model for capillary exchange. Am J Physiol Heart Circ Physiol 1966;210:1299–303.

[9] Sawada Y, Patlak CS, Blasberg RG. Kinetic analysis of cerebrovascular transport based on indicator diffusion technique. Am J Physiol 1989;256:H794–812.

[10] Moran GR, Prato FS. Modeling tissue contrast agent concentration: a solution to the tissue homogeneity model using a simulated arterial input function. Magn Reson Med 2001;45:42–5.

[11] Garpebring A, Ostlund N, Karlsson M, Östlund N. a Novel Estimation Method for Physiological Parameters in Dynamic Contrast-Enhanced MRI: Application of a Distributed Parameter Model Using Fourier-Domain Calculations. IEEE Trans Med Imaging 2009;{28}:1375–83.

[12] St. Lawrence KS, Lee T-Y. An Adiabatic Approximation to the Tissue Homogeneity Model for Water Exchange in the Brain: I. Theoretical Derivation. J Cereb Blood Flow Metab 1998;18:1365–77.

[13] Sangren WC, Sheppard CW. a mathematical derivation of the exchange of a labeled substance between a liquid flowing in a vessel and an external compartment. Bull Math Biophys 1953;15:387–94.

[14] Larson KB, Markham J, Raichle ME. Tracer-kinetic models for measuring cerebral blood flow using externally detected radiotracers. J Cereb Blood Flow Metab 1987;7:443–63.

[15] Koh TS, Zeman V, Darko J, Lee T-YY, Milosevic MF, Haider M, et al. the inclusion of capillary distribution in the adiabatic tissue homogeneity model of blood flow. Phys Med Biol 2001;46:1519–38.
[16] Koh TS, Cheong LHD, Tan CKM, Lim CCT. a distributed parameter model of cerebral blood-tissue exchange with account of capillary transit time distribution. Neuroimage 2006;30:426–35.
[17] Schabel MC. a unified impulse response model for DCE-MRI. Magn Reson Med 2012;68:1632–46.
[18] Weinmann HJ, Laniado M, Mützel W. Pharmacokinetics of GdDTPA/dimeglumine after intravenous injection into healthy volunteers. Physiol Chem Phys Med NMR 1984;16:167–72.
[19] Orton MR, D'Arcy JA, Walker-Samuel S, Hawkes DJ, Atkinson D, Collins DJ, et al. Computationally efficient vascular input function models for quantitative kinetic modelling using DCE-MRI. Phys Med Biol 2008;53:1225–39.
[20] Port RE, Knopp M V, Brix G. Dynamic contrast-enhanced MRI using Gd-DTPA: interindividual variability of the arterial input function and consequences for the assessment of kinetics in tumors. Magn Reson Med 2001;45:1030–8.
[21] Mcgrath DM, Bradley DP, Tessier JL, Lacey T, Taylor CJ, Parker GJM. Comparison of model-based arterial input functions for dynamic contrast-enhanced MRI in tumor bearing rats. Magn Reson Med 2009;61:1173–84.
[22] Parker GJM, Roberts C, Macdonald A, Buonaccorsi GA, Cheung S, Buckley DL, et al. Experimentally-derived functional form for a population-averaged high-temporal-resolution arterial input function for dynamic contrast-enhanced MRI. Magn Reson Med 2006;56:993–1000.
[23] Calamante F, Yim PJ, Cebral JR. Estimation of bolus dispersion effects in perfusion MRI using image-based computational fluid dynamics. Neuroimage 2003;19:341–53.
[24] Koh TS, Cheong DLH, Hou Z. Issues of discontinuity in the impulse residue function for deconvolution analysis of dynamic contrast-enhanced MRI data. Magn Reson Med 2011;66:886–92.
[25] Garpebring A. Contributions to quantitative dynamic contrast-enhanced MRI. [Thesis]. Umeå: Umeå Universitet; 2011. Umeå University medical dissertations, 1457.
[26] Aime S, Caravan P. Biodistribution of gadolinium-based contrast agents, including gadolinium deposition. J Magn Reson Imaging 2009;30:1259–67.
[27] Chan K, Wong W. Small molecular gadolinium(III) complexes as MRI contrast agents for diagnostic imaging. Coord Chem Rev 2007;251:2428–51.
[28] Heilmann M, Kiessling F, Enderlin M, Schad LR. Determination of pharmacokinetic parameters in DCE MRI: Consequence of nonlinearity between contrast agent concentration and signal intensity. Invest Radiol 2006;41:536–43.

[29] Schabel MC, Parker DL. Uncertainty and bias in contrast concentration measurements using spoiled gradient echo pulse sequences. Phys Med Biol 2008;53:2345–73.
[30] Jackson A, Buckley DL, Parker GJM. Dynamic Contrast-Enhanced Magnetic Resonance Imaging in Oncology. Springer; 2005.
[31] Schabel MC, Morrell GR. Uncertainty in T(1) mapping using the variable flip angle method with two flip angles. Phys Med Biol 2009;54:N1–8.
[32] Chang L-C, Koay CG, Basser PJ, Pierpaoli C. Linear least-squares method for unbiased estimation of T1 from SPGR signals. Magn Reson Med 2008;60:496–501.
[33] Kjolby BF, Mikkelsen IK, Pedersen M, Ostergaard L, Kiselev VG. Analysis of partial volume effects on arterial input functions using gradient echo: a simulation study. Magn Reson Med 2009;61(6):1300–9.
[34] Garpebring A, Wirestam R, Ostlund N, Karlsson M. Effects of inflow and radiofrequency spoiling on the arterial input function in dynamic contrast-enhanced MRI: a combined phantom and simulation study. Magn Reson Med 2011;65:1670–9.
[35] Yang C, Karczmar GS, Medved M, Stadler WM. Multiple reference tissue method for contrast agent arterial input function estimation. Magn Reson Med 2007;58:1266–75.
[36] Fluckiger JU, Schabel MC, Di Bella EVR. Model-based blind estimation of kinetic parameters in dynamic contrast enhanced (DCE)-MRI. Magn Reson Med 2009;62:1477–86.
[37] Schabel MC, Fluckiger JU, Di Bella EVR. a model-constrained Monte Carlo method for blind arterial input function estimation in dynamic contrast-enhanced MRI: I. Simulations. Phys Med Biol 2010;55:4783–806.
[38] Schabel MC, Di Bella EVR, Jensen RL, Salzman KL. a model-constrained Monte Carlo method for blind arterial input function estimation in dynamic contrast-enhanced MRI: II. In vivo results. Phys Med Biol 2010;55:4807–23.
[39] Keunen O, Taxt T, Bartoš M, Jiřík R, Thorsen F, Johansson M, Oudin A, Sanzey M, Abdulrahim S, Fack F, Bjerkvig R, Niclou S. Multi-modal imaging and pharmacokinetic modeling shed light on mechanism of action of anti-angiogenic therapy in malignant gliomas. Methods and Applications in Bioinformatics: From ideas to results. 2010, p. 3–4.
[40] De Naeyer D, De Deene Y, Ceelen WP, Segers P, Verdonck P. Precision analysis of kinetic modelling estimates in dynamic contrast enhanced MRI. MAGMA 2011;24:51–66.
[41] Seber GAF, Wild CJ. Nonlinear Regression (Wiley Series in Probability and Statistics). Wiley-Interscience; 2003.
[42] Fluckiger JU, Schabel MC, Di Bella EVR. Constrained estimation of the arterial input function for myocardial perfusion cardiovascular magnetic resonance. Magn Reson Med 2011;66:419–27.

[43] Fluckiger JU, Benefield BC, Harris KR, Lee DC. Absolute quantification of myocardial blood flow with constrained estimation of the arterial input function. J Magn Reson Imaging 2013;38:603–9.
[44] Kratochvíla J, Jiřík R, Bartoš M, Standara M, Starčuk Z, Taxt T. DCATH Model in Parametric Multi-Channel Blind AIF Estimation Using Dynamic Contrast-Enhanced MRI. To be submited to Magn Reson Imaging 2014
[45] Kratochvíla J, Jiřík R, Standara M, Bartoš M, Taxt T, Starčuk Z. Blind Parametric Multi-Channel Deconvolution for Estimation of Arterial Input Function in Dynamic Contrast-Enhanced MRI. In: ESMRB 2012 Congress, Book of Abstracts; 2012, p. 228–229.
[46] Østergaard L, Weisskoff RM, Chesler DA, Gyldensted C, Rosen BR. High resolution measurement of cerebral blood flow using intravascular tracer bolus passages. Part I: Mathematical approach and statistical analysis. Magn Reson Med 1996;36:715–25.
[47] Wirestam R, Andersson L, Ostergaard L, Bolling M, Aunola JP, Lindgren A, et al. Assessment of regional cerebral blood flow by dynamic susceptibility contrast MRI using different deconvolution techniques. Magn Reson Med 2000;43:691–700.
[48] Grüner R, Bjørnarå BT, Moen G, Taxt T. Magnetic resonance brain perfusion imaging with voxel-specific arterial input functions. J Magn Reson Imaging 2006;23:273–84.
[49] Larsson HBW, Hansen AE, Berg HK, Rostrup E, Haraldseth O. Dynamic contrast-enhanced quantitative perfusion measurement of the brain using T1-weighted MRI at 3T. J Magn Reson Imaging 2008;27:754–62.
[50] Griebel J, Pahernik S, Lucht R, DeVries A, Englmeier K, Dellian M. Perfusion and permeability: can both parameters be evaluated separately from dynamic MR data. ISMRM Proc 2001;9:2001–2001.
[51] Keeling SL, Bammer R, Kogler T, Stollberger R, 2004. On the convolution model of dynamic contrast enhanced magnetic resonance imaging and non-parametric deconvolution approaches. Special Research Center Report 298, University of Graz, Austria.
[52] Schmid VJ, Whitcher B, Padhani AR, Yang G-Z. Quantitative analysis of dynamic contrast-enhanced MR images based on Bayesian P-splines. IEEE Trans Med Imaging 2009;28:789–98.
[53] Keeling SL, Bammer R, Stollberger R. Revision of the theory of tracer transport and the convolution model of dynamic contrast enhanced magnetic resonance imaging. J Math Biol 2007;55:389–411.
[54] Keeling SL, Kogler T, Stollberger R. Deconvolution for DCE-MRI using an exponential approximation basis. Med Image Anal 2009;13:80–90.
[55] Bartoš M, Jiřík R, Taxt T. Comparison of Non-Blind and Blind Deconvolution by Richardson-Lucy Algorithm in MR Perfusion Imaging. Anal. Biomed. Signals Images, 2008, p. 47–8.

[56] Jiřík R, Souček K, Mézl M, Bartoš M, Dražanová E, Dráfi F, Grossová L, Kratochvíla J, Macíček O, Nylund K, Hampl A, Gilja O, Taxt T, Starčuk Z. Blind Deconvolution in Dynamic Contrast-Enhanced MRI and Ultrasound. In 36th Annual International Conference of the IEEE Engineering in Medicine and Biology Society. 2014. p. 4276 - 4279.
[57] Jiřík R, Souček K, Dražanová E, Grossová L, Standara M, Kratochvíla J, Macíček O, Malá A, Taxt T, Starčuk Z. Blind Mulitchannel Deconvolution for Estimation of a Parametric AIF in DCE-MRI of Mice. Proceedings of the International Society for Magnetic Resonance in Medicine 2014. Milano. 2014. p. 2754 - 2754.